Scene illuminant classification: brighter is better

Shoji Tominaga and Satoru Ebisui

Department of Engineering Informatics, Osaka Electro-Communication University, Neyagawa, Osaka 572-8530, Japan

Brian A. Wandell

Image Systems Engineering, Stanford University, Stanford, California 94305

Received January 3, 2000; revised manuscript received July 11, 2000; accepted July 28, 2000

Knowledge of the scene illuminant spectral power distribution is useful for many imaging applications, such as color image reproduction and automatic algorithms for image database applications. In many applications accurate spectral characterization of the illuminant is impossible because the input device acquires only three spectral samples. In such applications it is sensible to set a more limited objective of classifying the illuminant as belonging to one of several likely types. We describe a data set of natural images with measured illuminants for testing illuminant classification algorithms. One simple type of algorithm is described and evaluated by using the new data set. The empirical measurements show that illuminant information is more reliable in bright regions than in dark regions. Theoretical predictions of the algorithm's classification performance with respect to scene illuminant blackbody color temperature are tested and confirmed by using the natural-image data set.

OCIS code: 330.1690.

1. INTRODUCTION

The estimation of scene illumination from image data is important in several color engineering applications. In one application, color balancing for image reproduction, data acquired under one illuminant are rendered under a second (different) illuminant. A satisfactory color reproduction requires transforming the captured data, prior to display, to account for the illumination difference. Hence knowledge about the original scene illumination is a key step in the process. A second application is image database retrieval. Objects with different colors can produce the same image data when captured under different illuminants. Hence accurately retrieving objects on the basis of color requires an estimate of the scene illuminant.

Here we report two new contributions to the work on illuminant classification. First, we introduce an empirical data set of natural images that can be used to test illuminant classification algorithms.[1] Second, we review and evaluate some simple approaches to summarizing scene illumination. We focus on one method, which we call sensor correlation, and describe some of its strengths and weaknesses with respect to classifying illuminants of natural images.

2. BACKGROUND

Because of its significance, the theory of illuminant estimation has a long history in the fields of color science, image understanding, and image processing. A variety of methods for estimating the illuminant spectral power distribution have been proposed, and each assumes that there are significant physical constraints on the set of possible illuminant spectra.

Several illuminant estimation algorithms have expressed the physical constraint by assuming that the potential spectra fall within a low-dimensional linear model. The approach is useful in cases when the set of possible spectral power distributions are well characterized, such as daylight illuminants.[2] Linear models represent strong *a priori* information about the image illuminants, and accepting this knowledge in the form of a linear model allows the development of simple estimation algorithms.[3–9] A shortcoming of linear models is that they always include illuminants that are physically nonrealizable or unlikely to arise in practice. Many simple linear estimation procedures do not exclude such solutions, and in the presence of significant sensor noise poor performance can result. Brainard and Freeman[9] carefully state and analyze a Bayesian analysis of the problem that substantially improves upon the original formulation.

Finlayson *et al.*[10] suggest another interesting approach to the problem. (We refer to their collection of papers as FHH.) They begin with the assumption that the scene illuminant is one of a relatively small number of likely illuminants, such as the variety of daylight and indoor conditions in which images are acquired. Rather than estimating the spectral power distribution of the illuminant, the algorithm chooses the most likely scene illuminant from a fixed set. Classification rather than estimation is appropriate for applications, such as photography, when the vast majority of images are very likely to be captured under one of a small set of scene illuminants.

In describing their algorithms, FHH emphasize two properties. First, the illuminant is chosen by a simple correlation between a summary of the image data and a precomputed statistic that characterizes each illuminant. In fact, the algorithm draws its name, "Color by Correla-

tion," from this operation. Second, the algorithm operates on a chromaticity representation of the data (see Ref. 11, p. 1034). Hence we refer to FHH's method as chromaticity correlation.

Nearly all of the descriptions of the chromaticity correlation method are based on simulations, and these simulations do not include many features of natural images or real cameras. As part of our work on illuminant estimation, we decided to acquire a set of natural images and measure the correlated color temperature to summarize the scene illuminant. Here we describe the data set and report on our experimental results. These analyses have led us to propose modifications of the algorithm that we think are essential for classifying scene illuminants accurately.

3. EXPERIMENTAL METHODS

A. Image Capture

The image data used in these experiments were obtained with a Minolta camera (RD-175). The spectral responsivities of this camera were measured in separate experiments with a monochromator (see, e.g., Ref. 8). Like most modern cameras, the Minolta camera includes special-purpose processing to transform the sensor data prior to output. For the experiments described here, this processing was disabled.

When the camera is operated in this way, the transduction curve that relates input intensity to digital count is linear for the three sensor types. It is still possible, however, to adjust the sensor gain into one of two different modes. Figure 1 shows the spectral-sensitivity functions of the camera in these two modes. In one mode, appropriate for imaging under tungsten illumination (say, illuminant A), the blue-sensor gain is high. In a second mode, appropriate for imaging under daylight (D65), the blue-sensor gain is much lower. As we describe below, operating in the high blue-sensor gain improves the performance of the scene illuminant classification. Hence all analyses were performed in this mode. The images rendered as examples below have been color balanced only for display purposes.

At the time of image acquisition, we estimated the scene illuminant color temperature by placing a reference white in the scene and measuring the reflected light with a spectroradiometer. The correlated color temperature T_m can be determined from the CIE (x, y) chromaticity coordinates of the measured spectrum by using standard methods (Wyszecki and Stiles,[12], p. 225). Specification of a single color temperature for a complex scene is only an approximation to the complex spatial structure of the illuminant. Given that the goal of the classification is to provide a single estimate of the color temperature, this empirical approximation is a necessary starting point. Methods for improving this approximation will be taken up in Section 6.

Although they are not critical for this study, it is interesting to note that the Minolta camera includes three CCD sensor arrays. One array contains a striped pattern of red and blue sensors, and the other two arrays comprise green sensors that are slightly shifted in the image plane. This arrangement provides high spatial resolution for the green data set. The red and blue sensors were interpolated linearly and were combined with the green data in the analyses of this paper.

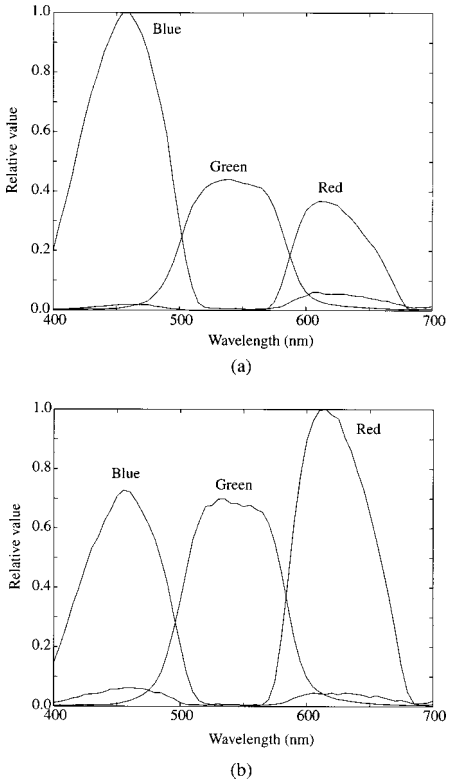

Fig. 1. Spectral-sensitivity functions of a camera: (a) tungsten mode, (b) daylight mode.

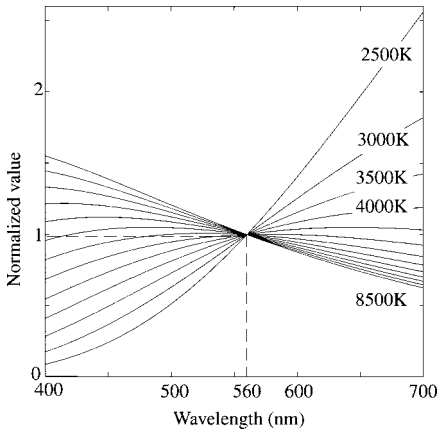

Fig. 2. Spectral power distributions of black body radiators.

Finally, to improve the quality of the measured images, each image was acquired along with a dark frame of the same exposure duration. The dark-frame values were measured and subtracted from every measured image to reduce the effects of read noise in the sensors.

B. Illuminant Set

The scene illuminants chosen for classification were blackbody radiators at color temperatures spanning 2500–8500 K in 500-K increments. Blackbody radiators are used frequently to approximate scene illuminants in

commercial imaging. Although the blackbody radiators are defined by a single parameter, color temperature, the spectral power distributions of these illuminants are not well described by a one-dimensional linear model (see Fig. 2). The equation of the spectral radiant power of the blackbody radiators as a function of temperature T (in kelvins) is given by the formula[12]

$$M(\lambda) = c_1\lambda^{-5}[\exp(c_2/\lambda T) - 1]^{-1}, \quad (1)$$

where $c_1 = 3.7418 \times 10^{-16}$ Wm^2, $c_2 = 1.4388 \times 10^{-2}$ m K, and λ is wavelength (m). The set of blackbody radiators includes sources whose spectral power distributions are close to CIE standard lights commonly used in color rendering, namely, illuminant A (an incandescent lamp with 2856 K) and D65 (daylight with a correlated color temperature of 6504 K).

In this paper the blackbody radiators are used not to illuminate natural scenes but to calibrate the measuring system and estimate the illuminant.

4. COMPUTATIONAL METHODS

A. Illuminant Gamut

The scene illuminant classification algorithms described here use a set of illuminant gamuts to define the range of sensor responses. The illuminant gamuts capture *a priori* knowledge about the illuminants. One precomputes the gamuts by choosing a representative set of surfaces and predicting the camera response to these surfaces under each illuminant. The illuminant gamuts described below were created with a database of surface spectral reflectances made available by Vrhel *et al.*[13] together with the reflectances of the Macbeth Color Checker. The Vrhel database consists of 354 measured reflectance spectra of different materials collected from Munsell chips, paint chips, and natural products. The illuminant gamut may be made larger or smaller by selecting a different database of surface-reflectance functions.

The illuminant gamuts are computed with the three sensors described in Fig. 1. The sensor responses are predicted with

$$\begin{bmatrix} R \\ G \\ B \end{bmatrix} = \int_{400}^{700} S(\lambda)M(\lambda)\begin{bmatrix} r(\lambda) \\ g(\lambda) \\ b(\lambda) \end{bmatrix} d\lambda, \quad (2)$$

where $S(\lambda)$ is the surface spectral-reflectance function; $r(\lambda)$, $g(\lambda)$, and $b(\lambda)$ are the spectral-sensitivity functions; and $M(\lambda)$ is the blackbody radiator. These (R, G, B) values are used to define the illuminant gamuts with methods that are more fully described below.

Creation of the illuminant gamuts is a central part of the classification algorithms, and the engineer has some ability to structure the gamuts by choosing a coordinate frame and selecting the objects that will be used to represent typical surfaces. In general, the gamuts should satisfy two conflicting criteria. First, it is important that the illuminant gamuts provide good coverage of the measurement space. Second, when two illuminants require different image processing, it is desirable that the corresponding illuminant gamuts have little overlap. Small overlap between a pair of illuminant gamuts is an indicator that the algorithm should be able to discriminate well between the illuminant pair. In considering the illuminant classification algorithms, we have examined several coordinate systems with these criteria in mind.

Finlayson[11] used chromaticity coordinates to represent the gamuts: $(R/B, G/B, 1) = (r, g, 1)$. Like all chro-

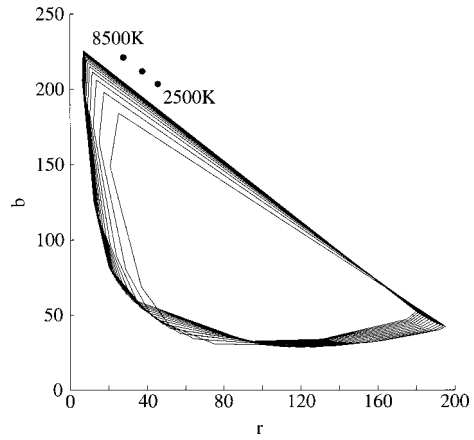

Fig. 3. Illuminant gamuts for blackbody radiators in the (r, b) chromaticity plane.

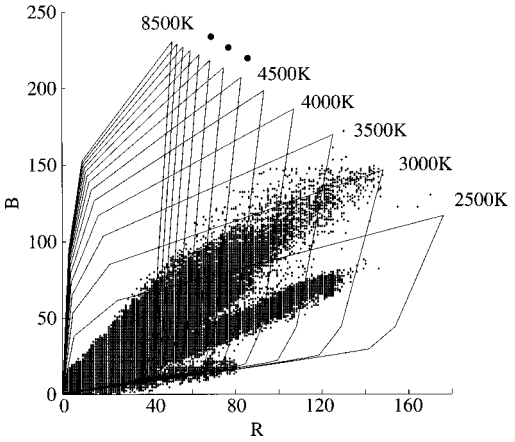

Fig. 4. Illuminant gamuts for blackbody radiators in the (R, B) sensor plane.

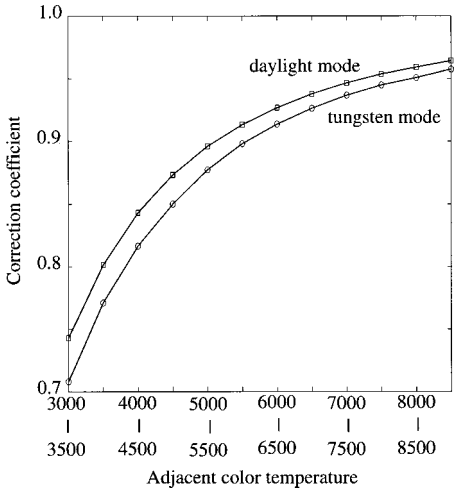

Fig. 5. Correlation coefficients between adjacent gamuts for the sensor sensitivity functions in Figs. 1(a) and 1(b).

maticity projections, measurements that differ only by a scalar intensity are collapsed to a common (r, g) coordinate, eliminating differences that are due to illuminant scaling. The boundary of this illuminant's gamut is obtained from the convex hull of the set of (r, g) points. This particular set of chromaticity coordinates requires division by the B-sensor value, and this can be problematic when the B sensor is near zero. A conventional chromaticity gamut using the sum of the three responses has less of a problem with the denominator, so we have experimented using the conventional form:

$$r = R/(R + G + B), \qquad b = B/(R + G + B). \quad (3)$$

Figure 3 shows a collection of illuminant gamuts for blackbody radiators and the Minolta camera chromaticities. The gamuts do cover most of the space, but the 8500-K gamut includes most of the area in the other gamuts. There is very little separation between illuminants that require different postprocessing, such as the 8500-K and 5000-K illuminants.

From inspecting these illuminant gamuts, we find that illuminant classification depends on the saturated colors that define the edges of gamuts on the chromaticity diagram. Objects in the data set that have relatively narrowband reflectance functions determine these chromaticity values. The number of photons scattered from such surfaces will be relatively low. Hence the presence of even modest amounts of sensor noise makes chromaticity coordinates a poor choice for illuminant classification. Moreover, the illuminant gamuts in the CIE *xy* chromaticity plane are presented in Ref. 14. Transforming the data to a device-independent coordinate system, such as CIE *XYZ*, does not improve the gamut separation or the signal-to-noise consideration. Moreover, note that transformation from the camera *RGB* to CIE *XYZ* is not always accurate.

The chromaticity representation removes intensity differences. This is not desirable because, in the natural data set that we have collected, high-intensity regions contain more illuminant information than do dark regions. To see why this might be possible, consider a black surface. The image of the surface will have close to a zero response under any illuminant, and its chromaticity coordinates will be determined mainly by system noise. A white surface, however, will map reliably to different chromaticities depending on the illuminant spectral power distribution. Combining the two measurements will produce worse classification than using the bright region alone.

This thought experiment provides a motivation for defining illuminant gamuts directly on the sensor data, say, in the *RB* plane. The (R, B) sensor plane is a reasonable choice for the blackbody radiators because their illuminant gamuts differ mainly with respect to this plane. Although there is nothing to preclude the use of all three sensor dimensions, for classifying blackbody radiators the (R, B) plane seems to be adequate. The key point is that using sensor space, rather than chromaticity coordinates, preserves relative intensity information that is helpful.

B. Image Scaling

The main difficulty with using the sensor data is the presence of overall intensity differences among images. The data can be adjusted by a simple scaling operation, equivalent to placing a neutral density filter in the light path or adjusting the exposure duration. Such a scaling operation preserves the shape of the image gamut and the relative intensity information within an image. To scale the data, we define I_i as the ith pixel intensity,

$$I_i = (R_i^2 + G_i^2 + B_i^2)^{1/2}, \quad (4)$$

and let $I_{\max}$ be the maximal value of the intensity over the image. Then to scale the intensity across different images, we divide the sensor *RGB* values by the maximum intensity,

$$(R, G, B) = (R/I_{\max}, G/I_{\max}, B/I_{\max}). \quad (5)$$

As a practical matter, the choice of a maximum-intensity pixel should be stable, making the normalization reliable. To improve stability, we normalized image intensities using a bright cluster, not just an isolated bright pixel. This procedure was enforced by representing the data in the (R, G, B) volume and choosing the brightest pixel (R_b, G_b, B_b) in a cluster with more than 16 pixels greater than $R_b - 5$, $G_b - 5$, and $B_b - 5$. In the above operation, we exclude all saturated pixels prior to the calculation.

The boundary of the illuminant gamut is obtained from the convex hull of the set of (R, B) points. Figure 4 shows the illuminant gamuts of the blackbody radiators in the (R, B) plane. These illuminant gamuts are better

Fig. 6. Example of a natural scene.

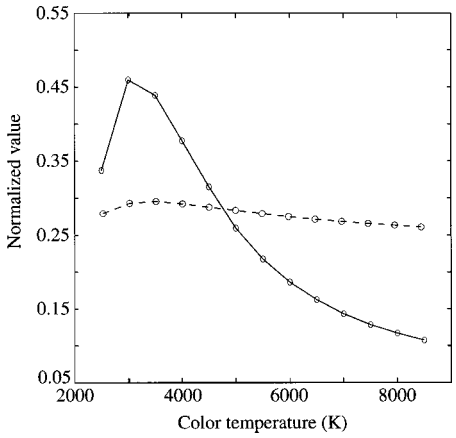

Fig. 7. Correlation function for the image shown in Fig. 6. The solid and the dashed curves represent, respectively, the proposed sensor correlation and the chromaticity correlation.

Fig. 8. Set of 14 images of indoor scenes under an incandescent lamp.

separated than those in the chromaticity plane, and the best separation occurs for high-intensity values. As we will confirm experimentally, the dark regions contribute no significant information to the classification choice and do not limit performance in this plane. The gamut in the sensor space comes to a point at the high end, so that no matter what surfaces are in the image, the most intense regions track the illuminant variation better.

C. Image and Gamut Correlation

To quantify the overlap, either between image data and illuminant gamuts or between a pair of gamuts, we calculate the correlation suggested by FHH. The RB plane is divided into a regular grid (i, j) with small even intervals (usually 256×256). The illuminant gamuts are represented by setting a $g(i, j)$ value to 1 or 0 depending on whether the cell falls inside the convex hull. The gamut

correlation coefficient is a useful figure of merit for evaluating the ability of different sensor classes to separate illuminants.

A correlation value can be computed between a pair of illuminant gamuts with use of the standard formula,

$$\mathrm{Cor} = \sum_{i,j} x_{ij} y_{ij} \Big/ \left[\left(\sum_{i,j} x_{ij}^2 \right) \left(\sum_{i,j} y_{ij}^2 \right) \right]^{1/2}, \qquad (6)$$

where x_{ij} and y_{ij} are indicator variables for the gamuts x and y: The value x_{ij} is 1 if (i, j) are inside the gamut and 0 otherwise. Figure 5 shows the correlation coefficients for the sensor sensitivity functions in Figs. 1(a) and 1(b). Because the correlation is lower for the high blue-sensor gain setting, we used this mode.

For the correlation between an image and illuminant gamuts, the image data are mapped into an array of cells with the same size as $g(i, j)$. In this case the image data are converted to the binary histogram with possible holes. For an efficient correlation computation, we used the following computational procedure.

The 13 illuminant gamuts were represented by a single 256×256 array $\mathbf{M}[R][B]$. Let $M_i[R][B]$ be the ith bit of $\mathbf{M}[R][B]$. We set $M_i[R][B]$ to 1 if (R, B) is inside the ith illuminant gamut and 0 otherwise. The correlation between an image and each of the illuminant gamuts can be computed by summing the binary values on the gamut array corresponding to the (R, B) pixel values. This binary computation includes neither multiplication nor conditional statement. The integer counter vector C_i is initialized to 0. Then, for each scaled image pixel, (R, B), the correlation of the image with the ith gamut is computed as

```
For all image pixels, (R, B)
  For i = 1:13
    C_i = C_i + M_i[R][B]
    M_i[R][B] = 0
  end
end.
```

The counter C_i never exceeds 256×256. The illuminant is classified into the category with the largest value of C_i.

5. EXPERIMENTAL RESULTS

The illuminant classification algorithm is illustrated by applying it to the image in Fig. 6. This image was acquired indoors under a calibrated light source with correlated color temperature near 3000 K. The scaled (R, B) values from the image are plotted as the points overlying the illuminant gamuts in Fig. 4 (a small number of saturated pixels on the picture frame in the upper left are excluded). The sensor values, particularly for high luminance levels, fit selectively within the gamut of 3000 K. The few points outside the gamut are due to the specular highlights on the back wall and some points on the blue striped shirt that fluoresce.

Figure 7 shows the correlation between the image data and each of the illuminant gamuts. The solid curve represents the correlation function obtained by the proposed sensor correlation method. Corresponding to the image of the points and illuminant gamuts, the peak correlation is at a color temperature of 3000 K. The correlation graph is quite selective, clearly identifying 3000 K as the peak. The dashed curve in Fig. 7 represents the results obtained by the chromaticity correlation method with use of the gamut in Fig. 3. The correlation function is so flat that we cannot select a unique peak.

We have evaluated the sensor correlation algorithm using a database of images that include both indoor and outdoor scenes. Figure 8 shows a set of 14 images of scenes photographed under an incandescent lamp in our laboratory. Figure 9 shows the correlation functions of each of the images. The solid and the dashed curves represent, respectively, the proposed sensor correlation and the chromaticity correlation. The estimated illuminant color temperatures obtained by the sensor correlation are coincident as 3000 K for all images.

Figure 10 shows a set of images acquired outdoors under a cloudy sky. The correlation functions for these images are shown in Fig. 11, where the solid and the dashed curves represent, respectively, the sensor correlation and the chromaticity correlation. The color temperatures obtained by the sensor correlation are estimated in the range of 5000–6000 K. On the other hand the chromaticity correlation did not provide meaningful estimates. The direct measurements of color temperature in outdoor scenes vary somewhat over time and also with the viewing direction of the reference white placed in the scene to measure the scene illuminant, but the measurements for the above scene ranged from 5500 to 6000 K. A low color temperature estimate of 5000 K was made for image 5. The roof in that scene is transparent, so the boards under the roof are illuminated with a different color temperature from the global scene illuminant.

There are several ways to measure the performance of the classification algorithm. First, the mean error between the estimated and the measured color temperature is 124 K for the indoor scenes and 415 K for the outdoor scene. Second, the color temperature errors can be expressed as a range of spectral power distributions, and these are shown in Fig. 12, where the solid curves represent the estimated spectral distributions by the blackbody radiators and the dashed curves represent the average curves of the full spectra of the measured illuminants.

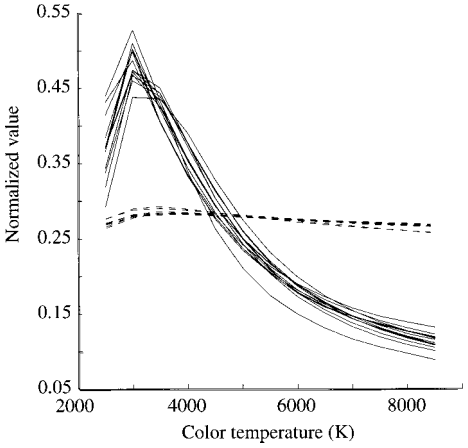

Fig. 9. Set of correlation functions for the indoor images. The solid and the dashed curves represent, respectively, the sensor correlation and the chromaticity correlation.

Fig. 10. Set of images of outdoor scenes.

When the illuminants are measured in this way, the error for the indoor scenes is smaller than the error for the outdoor scenes. Third, the spectral-power-distribution differences can be expressed as CIELAB color differences with respect to the average surface. Specifically, let $M_e(\lambda)$ and $M_m(\lambda)$, respectively, be the estimated and the measured spectral power distributions of a blackbody radiator spectrum, and let $S_a(\lambda)$ be the average surface spectral reflectance in the surface database. From these curves and Eq. (2) we can predict sensor responses to the average surface under two illuminants. Then we can linearly transform the sensor values to estimate CIE *XYZ* values and finally to CIE-L*a*b* values. From these values, the mean errors are $\Delta E_{ab} = 10.26$ for the indoor scenes and $\Delta E_{ab} = 8.05$ for the outdoor scenes. The errors in the chromaticity (a*, b*) are 2.17 and 1.12, respectively. The results for the outdoor scenes are better than those for the indoor scenes. It should be noted that error

in the color temperature scale does not always correspond to color difference in the perceptually uniform scale.

For the images that we have measured, data in the bright regions of the image are decisive in discriminating between the illuminants. Figure 13 shows the image data points grouped according to intensity for the sample scene in Fig. 6. The five types labeled a, b ,... , e in the histogram show five intensity ranges, corresponding to the percentiles 0–20, 20–40, and so forth. The top 20% of pixel intensities are shown in Fig. 14. These points are part of the human faces, a part of wall, a shirt, and a sweater.

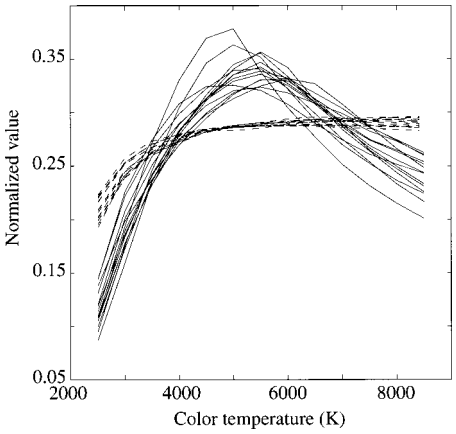

Fig. 11. Set of correlation functions for the outdoor images. The solid and the dashed curves represent, respectively, the sensor correlation and the chromaticity correlation.

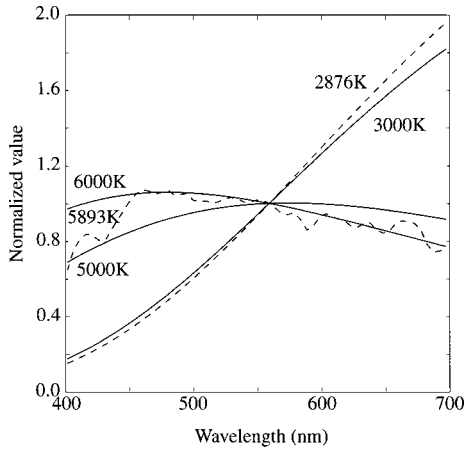

Fig. 12. Color temperature errors as a range of spectral power distribution. The solid curves represent the estimated spectral distribution, and the dashed curves represent the average full spectra of the measured illuminants.

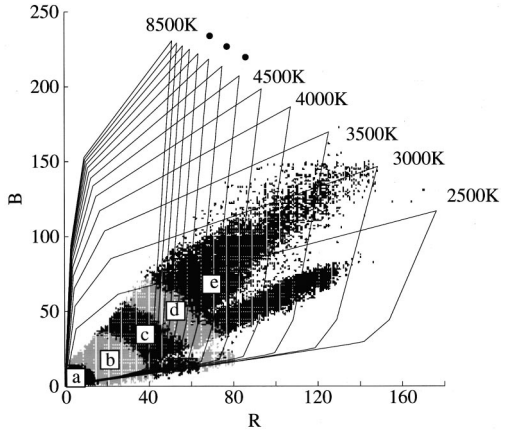

Fig. 13. Image data points grouped according to intensity for the natural scene in Fig. 6. The five types of labeled a,b ,..., e represent five intensity ranges, corresponding to the percentiles 0–20, 20–40, and so forth.

Fig. 14. Binary image showing the top 20% of pixel intensities in the natural scene.

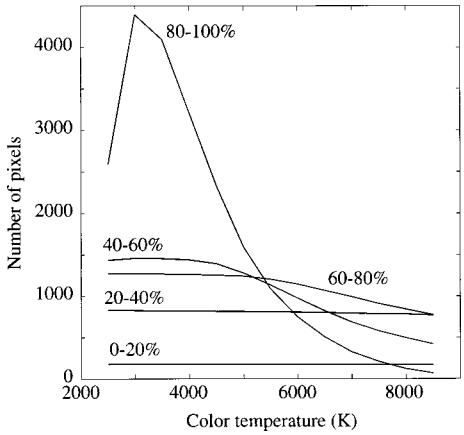

Fig. 15. Set of correlation functions calculated separately for each of the intensity ranges.

Correlation functions measured separately for each of these intensity ranges are shown in Fig. 15. The correlation function becomes sharper as the brightness level increases. The brightest 20% of the pixels is enough to estimate the color temperature, and the remaining dark regions do not contribute significantly.

6. DISCUSSION

We have described experiments with a modest classification goal: to summarize the illuminant color temperature in indoor and outdoor natural images. The results are correspondingly simple: For the images that we have collected, illuminants are well classified by comparing the values of the red- and blue-sensor values measured from relatively light surfaces. For the camera and range of illumination conditions tested here, the sensor correlation classified blackbody radiators to within a few hundred degrees kelvin.

A. Sensor Values and Chromaticity Coordinates

Basing the classification algorithm on image sensor values improved performance compared with basing it on image chromaticity coordinates. A graphic illustration of

why this might be possible is shown in Fig. 16. This image illustrates the difference between sensor values and chromaticity coordinates using a simple two-dimensional graphical example. Panel (a) shows three image points in the (R, B) sensor plane. These points are plotted as chromaticity coordinates, so the original sensor measurements could have been made at any of the values indicated by the dashed lines. Panel (b) shows two possible distributions of the original data. The left graph shows a distribution in which the chromaticity coordinates of points with relatively large blue-sensor responses are more intense. This pattern of responses would be expected under a blue-sky illumination. The right graph shows a distribution in which the chromaticity coordinates of points with relatively large red-sensor values are more intense. This pattern of responses would be expected under a tungsten illumination. It is straightforward to distinguish the intensity information, shown by the position of the points in the left and right graphs of panel (b), under high and low color temperatures. When the analysis begins with chromaticity coordinates, this relative intensity information is unavailable.

B. Surface Shape and Illuminant Distribution

Forsyth first introduced the canonical sensor space gamut.[15] The analysis developed in that paper included the assumption that surfaces are flat and that the illuminant does not vary over space. This might cause some concern in applying the algorithm to natural images, yet we have observed that neither assumption is essential to the classification method. Surface-reflectance scaling by geometric changes and illuminant intensity scaling by shading variation leave the convex hull of the sensor gamut unchanged. Both of these effects (illumination scaling and variations in surface orientation) are present in the test images, and neither effect challenges the algorithm.

C. Limitations

The experiments and methods that we have described have several limitations. Overcoming certain of these limitations will require additional work, but a solution can be foreseen. For example, we have performed our calculations using only two of the three color channels. This limitation could be lifted at the cost of increased computation. Also, the selection of surfaces for defining the gamut should be refined and based on better information regarding typical pictorial content. It is also possible to introduce Bayesian methods into the computational procedure. The cost of using a more complex algorithm, and the difficulty in identifying the probabilities of observing illuminants and surfaces within an image, must be weighed against the benefits of including such processing.

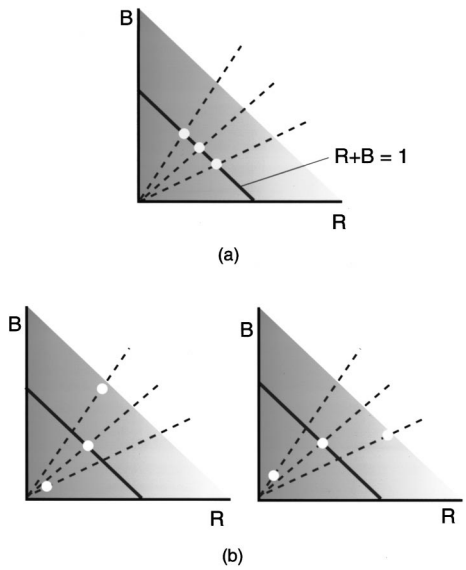

Fig. 16. Graphical example illustrating the difference between sensor values and chromaticity coordinates.

The most serious limitation, however, concerns the implicit model of the scene. Although the use of a single color temperature to characterize the scene illuminant is a reasonable starting point and is common practice in photography, the approximation is not accurate. Indirect illumination scattered from large objects in the scene, shadows, transparencies, and geometrical relationships between small light sources and surface orientation all make the image scene spatially complex. Identifying the complex pattern of the global illumination is needed for applications in computer-graphics rendering (see Ref. 16). But this complexity is well beyond the illumination estimates derived from the simple methods described here and serves only to raise additional research questions.

Finally, the classification method described here, like many others in common use, is vulnerable to variability in the collection of scene surfaces. For any illuminant it is possible to choose a collection of surfaces that will cause the algorithm to make incorrect classifications. This vulnerability is true of nearly all classification algorithms that have been proposed to date. Human perception appears to be less susceptible to this type of error (see, e.g., Ref. 17), and the size and potential significance of the gap between algorithm and human performance will be interesting to explore.

ACKNOWLEDGMENTS

This work was supported by Dainippon Screen MFG, Japan, and support was provided to the Stanford Programmable Digital Camera program by Agilent, Canon, Eastman Kodak, Hewlett-Packard, Intel, and Interval Research corporations. We thank Y. Nayatani, H. Hel-Or, M. Bax, J. DiCarlo, and J. Farrell for useful discussions and comments on the manuscript.

Address correspondence to Shoji Tominaga, Department of Engineering Informatics, Osaka Electro-Communication University, Neyagawa, Osaka 572-8530, Japan. E-mail, shoji@tmlab.osakac.ac.jp; phone, 81-72-820-4562; fax, 81-72-824-0014.

REFERENCES

1. The image data used in this paper will be available at http://www.osakac.ac.jp/labs/shoji/.
2. D. B. Judd, D. L. MacAdam, and W. S. Stiles, "Spectral distribution of typical daylight as a function of correlated color temperature," J. Opt. Soc. Am. **54**, 1031–1040 (1964).
3. L. T. Maloney and B. A. Wandell, "Color constancy: a method for recovering surface spectral reflectance," J. Opt. Soc. Am. A **3**, 29–33 (1986).

4. S. Tominaga and B. A. Wandell, "The standard surface reflectance model and illuminant estimation," J. Opt. Soc. Am. A **6**, 576–584 (1989).
5. B. V. Funt, M. S. Drew, and J. Ho, "Color constancy from mutual reflection," Int. J. Comput. Vis. **6**, 5–24 (1991).
6. M. D'Zmura and G. Iverson, "Color constancy: I. Basic theory of two-stage linear recovery of spectral descriptions for lights and surfaces," J. Opt. Soc. Am. A **10**, 2148–2165 (1993).
7. M. D'Zmura, G. Iverson, and B. Singer, "Probabilistic color constancy," in R. D. Luce *et al.*, eds., *Geometric Representations of Perceptual Phenomena* (Erlbaum, Mahway, N.J., 1995), pp. 187–202.
8. S. Tominaga, "Multichannel vision system for estimating surface and illumination functions," J. Opt. Soc. Am. A **13**, 2163–2173 (1996).
9. D. H. Brainard and W. T. Freeman, "Bayesian color constancy," J. Opt. Soc. Am. A **14**, 1393–1411 (1997).
10. G. D. Finlayson, P. M. Hubel, and S. Hordley, "Color by correlation," in *Proceedings of the Fifth Color Imaging Conference* (Society for Imaging Science and Technology, Springfield, Va., 1997), pp. 6–11.
11. G. D. Finlayson, "Color in perspective," IEEE Trans. Pattern Anal. Mach. Intell. **18**, 1034–1038 (1996).
12. G. Wyszecki and W. S. Stiles, *Color Science: Concepts and Methods, Quantitative Data and Formulae* (Wiley, New York, 1982).
13. M. J. Vrhel, R. Gershon, and L. S. Iwan, "Measurement and analysis of object reflectance spectra," Color Res. Appl. **19**, 4–9 (1994).
14. S. Tominaga, S. Ebisui, and B. A. Wandell, "Color temperature estimation of scene illumination," in *Proceedings of the Seventh Color Imaging Conference* (Society for Imaging Science and Technology, Springfield, Va., 1999), pp. 42–47.
15. D. A. Forstyth, "A novel algorithm for color constancy," Int. J. Comput. Vis. **5**, 5–36 (1990).
16. Y. Yu, P. Debevec, J. Malik, and T. Hawkins, "Inverse global illumination: recovering reflectance models of real scenes from photographs," Special Interest Group on Computer Graphics and Interactive Techniques (SIGGRAPH) **99**, 215–224 (1999).
17. D. H. Brainard, "Color constancy in the nearly natural image. 2. Achromatic loci," J. Opt. Soc. Am. A **15**, 307–325 (1998).